Document downloaded from:

http://hdl.handle.net/10251/192122

This paper must be cited as:

Garrido-García, EM.; Climent, E.; Marcos Martínez, MD.; Sancenón Galarza, F.; Rurack, K.; Martínez-Máñez, R. (2022). Dualplex lateral flow assay for simultaneous scopolamine and "cannibal drug" detection based on receptor-gated mesoporous nanoparticles. Nanoscale. 14(37):13505-13513. https://doi.org/10.1039/d2nr03325a

The final publication is available at

https://doi.org/10.1039/d2nr03325a

Copyright The Royal Society of Chemistry

Additional Information

ARTICLE

Selective dualplex lateral flow assay for simultaneous scopolamine and "cannibal drug" detection based on receptor-gated mesoporous nanoparticles

Eva Garrido,[abcd] Estela Climent,[e] M. Dolores Marcos,[abcd] Félix Sancenón,[abcd] Knut Rurack*[e] and Ramón Martínez-Máñez*[abcd]

We report herein the design of a strip-based rapid test utilizing bio-inspired hybrid nanomaterials for the *in situ* and *at site* detection of the drug scopolamine (SCP) using a smartphone for readout, allowing SCP identification in diluted saliva down to 40 nM in less than 15 min. For this purpose, we prepared a nanosensor based on mesoporous silica nanoparticles loaded with a fluorescent reporter (rhodamine B) and functionalized with bethanechol, a potent agonist of recombinant human muscarinic acetylcholine receptor M_2 (M_2-AChR). M_2-AChR interaction with the anchored bethanechol derivative leads to capping of the pores. The sensing mechanism relies on binding of SCP to M_2-AChR resulting in pore opening and delivery of the entrapped rhodamine B reporter. Moreover, the material was incorporated into strips for lateral-flow assays coupled to smartphone readout, giving fast response time, good selectivity, and exceptional sensitivity. In an attempt to a mobile analytical test system for law enforcement services, we have also developed a dualplex lateral flow assay for SCP and 3,4-methylenedioxypyrovalerone (MDPV) also known as the so-called "cannibal drug".

1. Introduction

Drug-facilitated sexual assault (DFSA) is a term used to define sexual assault without consent of the victim that is incapacitated and/or unable to provide approval to the sexual act as a result of administration a of psychoactive substance or drug cocktails usually without the permission of the victim.[1,2] In recent years, this phenomenon has acquired greater relevance worldwide and social impact fuelled by the significant increase in cases that already account for roughly 20.9% of sexually assaulted victims.[3] The psychoactive substance most commonly associated with DFSA is alcohol, yet the use of recreational drugs is rising as the drug market is expanding, providing faster and cheaper ways to disable the victim. Among psychoactive substances used in DFSA, γ-hydroxybutyric acid (GHB), 3,4-methylenedioxypyrovalerone (MDPV, also called "cannibal drug"), ketamine, flunitrazepam or scopolamine (SCP) are among the most noteworthy.

SCP, also known by the street name of "burundanga", has emerged as a perfect psychotropic substance for aggressors, as it induces an automatism in the brain of the victim that causes a state of submission. Chemically, SCP is an extremely toxic tropane alkaloid found as a secondary metabolite in certain plants of the Solanaceae family and for centuries it has been widely used for ritual and medical purposes.[4] Structurally, SCP is optically and biologically active, characterized by its unique bicyclic tropane ring system and its consumption produces potent psychotropic effects, including delirium-like states with hallucinations, altered mood, and cognitive deficits.[5] Pharmacological effects of SCP and their duration depend mainly on the format in which the drug is consumed, appearing within minutes for solutions, or elixirs (peaking at 15–60 min and lasting for 4 h) and within 20−30 min for capsules (peaking at 40–90 min and lasting for 12 h).[5] As a result of their powerful sedative-hypnotic effects, SCP has currently become well-known for being employed to commit crimes such as robbery, kidnapping and sexual assaults.[6,7] Biologically, SCP is a non-selective and non-competitive muscarinic acetylcholine receptor (M_1~M_5-AChR) antagonist with rapid and robust antidepressant effects in humans and other species.[8-10] Particularly, SCP is able to block or dampen the biological response of the acetylcholine receptor because it binds to an allosteric M_2-AChR site that is separate from the active recognition site of acetylcholine, inducing free acetylcholine levels to increase.

Owing to the increasing use of SCP in rape assaults as well as the broad diversification of new substances available on the underground market, an acute need has arisen to develop innovative and efficient analytical methods for the identification of DFSA substances. For SCP, a wide variety of techniques have been used for its reliable identification in different adulterated samples, such as gas chromatography,[11, 12] high-performance liquid chromatography[13,14] and capillary zone electrophoresis.[15] Most of these studies have been

[a.] *Instituto Interuniversitario de Investigación de Reconocimiento Molecular y Desarrollo Tecnológico (IDM), Universitat Politècnica de València, Universitat de València, Spain.*
[b.] *CIBER de Bioingeniería, Biomateriales y Nanomedicina (CIBER-BBN).*
[c.] *Unidad Mixta de Investigación en Nanomedicina y Sensores. Universitat Politècnica de València, Instituto de Investigación Sanitaria La Fe, Valencia, Spain.*
[d.] *Unidad Mixta UPV-CIPF de Investigación en Mecanismos de Enfermedades y Nanomedicina, Universitat Politècnica de València, Centro de Investigación Príncipe Felipe, Valencia, Spain.*
[e.] *Chemical and Optical Sensing Division, Bundesanstalt für Materialforschung und-prüfung (BAM) Richard-Willstätter-Str. 11, 12489, Berlin, Germany.*
†Electronic Supplementary Information (ESI) available: [details of any supplementary information available should be included here]. See DOI: 10.1039/x0xx00000x

Please do not adjust margins

focused on the determination of SCP in serum, plasma, and other biological samples, such as urine or hair.[16] However, these analytical techniques are commonly employed in a dedicated laboratory environment, requiring sophisticated instrumentation, and cannot be used in situ or at site. In this scenario, lateral flow assays (LFAs) have recently attracted a lot of attention due to their pocket-portable formats, short assay times, little interferences, low costs, and because they can be easy operated by non-specialized personnel. Moreover, LFAs can be designed to detect several compounds simultaneously by obtaining results in a short time showing high selectivity and sensitivity in the ppb range.[17,18]

From another viewpoint, gated mesoporous silica nanoparticles (MSNs) have raised considerable interest owing to the beneficial properties of the silica support such as high stability and rigidity, homogeneous and well-defined porosity (with diameters of 2–10 nm), high specific surface area and loading capacity, easily controllable morphology and tuneable surface chemistry.[19] Although gated MSNs have been widely used in drug delivery,[20,21] recently, the use of gated MSNs in sensing[22,23] and communication applications[24] has also become more popular. Sensing gated MSNs are composed of MSNs loaded for instance with selected fluorophores and functionalized with different supramolecular or biological assemblies (such as proteins,[25] enzymes,[24,26,27] antibodies,[28-30] and aptamers[31]) acting as 'molecular gates' (also known as gatekeepers or nanovalves). Gated MSNs show ideally "zero" release in the absence of an analyte, yet the presence of a target species induces, usually, a displacement of the capping ensemble, resulting in cargo delivery which is proportional to the analyte concentration. In addition, gated materials show inherent amplification features as just a few analyte molecules can induce the release of a large number of entrapped cargo molecules.[32] This led to a successful integration of gated MSN materials with fluorogenic response into LFAs with high sensitivity and selectivity for target analytes, demonstrating the tremendous potential of this approach for dipstick tests for a large range of applications.[33]

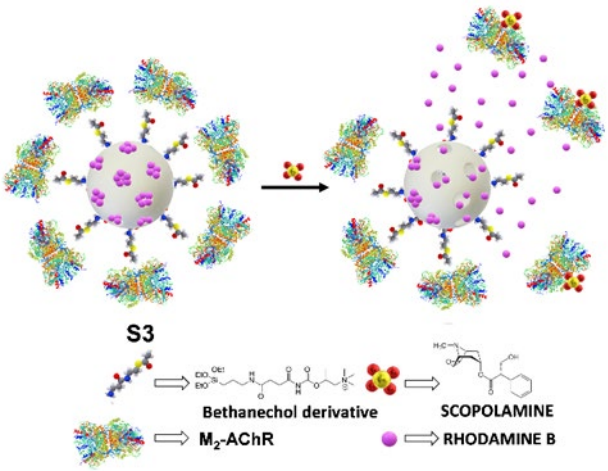

Scheme 1. Schematic of the uncapping mechanism for solid **S3** in the presence of SCP.

Based on the above, we report herein the design, preparation, and characterization of a nanosensor based on gated MSNs for SCP detection. The SCP nanosensor consists of capped MSNs loaded with rhodamine B that is selectively released in the presence of SCP in a sample, uncapping the ensemble. The nanoprobe shows a highly sensitivity in buffer solution and in a competitive environment such as saliva and is selective for SCP versus other common drugs. The SCP nanoprobe is incorporated into strips for lateral-flow assays coupled to smartphone readout, achieving a fast response and good selectivity and sensitivity. Taking into account the versatility of the gated material and the modularity of the assay, a dualplex lateral flow assay capable of detecting in situ and at site both, SCP and the so-called "cannibal drug" MDPV is also developed.

2. Results and discussion

The nanosensor design is depicted in Scheme 1. It consists of MSNs loaded with a fluorescent reporter (rhodamine B) and functionalised on the external surface with a bethanechol derivative (carbamyl-β-methylcholine chloride, also known as bethanechol) which is a non-selective muscarinic receptor agonist that increases the M_2-AChR activity.[34] In addition, the loaded system is finally capped by interaction between the grafted bethanechol derivative and M_2-AChR (**S3** in Scheme 1). For the M_2-AChR receptor, the reported dissociation constants of agonist binding (K_D) to bethanechol is 171 µM (for comparison it is 15.8 ± 3.8 µM for acetylcholine)[35] which explains the rationale behind the use of M_2-AChR for pore blocking.

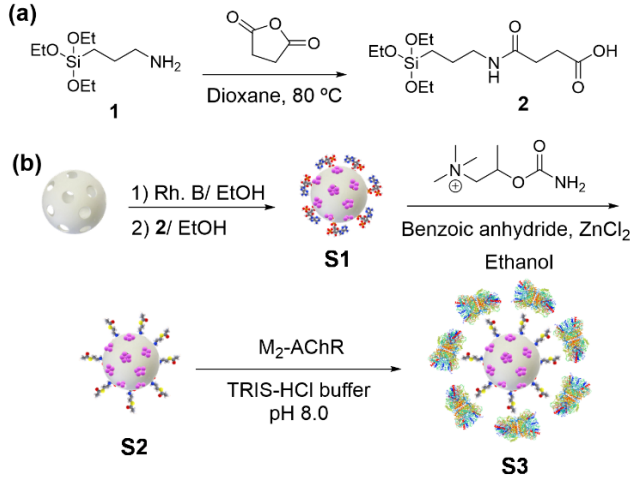

Scheme 2. Synthetic route to solid **S3**.

MSNs were prepared following reported procedures based on the condensation of tetraethyl orthosilicate (TEOS) in the presence of cetyltrimethylammonium bromide (CTAB) as micellar template. The as-made MSNs were calcinated at 550 °C for surfactant removal[36] and the empty pores were loaded with rhodamine B by soaking MSNs into an ethanolic solution of the fluorophore. Subsequently, the external surface of MSNs was functionalized with compound **2** yielding a pink solid (**S1**). Compound **2** was synthetised through the reaction between succinic anhydride and 3-(aminopropyl)triethoxysilane (**1**) using a previously described procedure (Scheme 2a).[37] In a next step, bethanechol chloride was

Please do not adjust margins

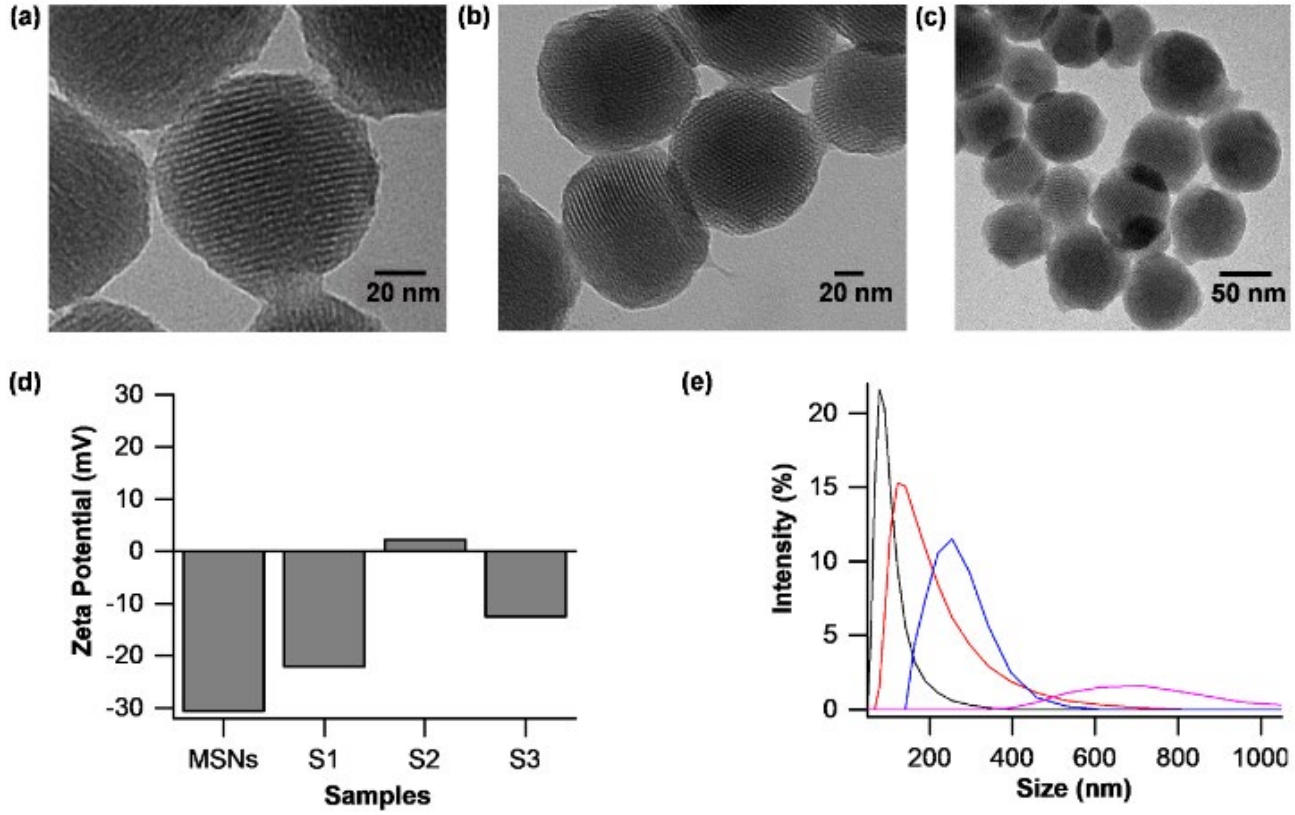

Figure 1. TEM images of (a) calcined MSNs, (b) **S2** and (c) **S3**, showing the typical porosity of the mesoporous silica matrix. (d) Zeta Potential for calcined MSNs, **S1**, **S2** and **S3**. (e) Hydrodynamic diameter distribution of calcined MSNs (black line), **S1** (red line), **S2** (blue line) and **S3** (pink line) determined by DLS.

grafted covalently to **2** on solid **S1** in the presence of benzoic anhydride and $ZnCl_2$,[38] giving solid **S2**. The final nanoprobe (**S3**) was obtained by stirring a suspension of **S2** in Tris-HCl buffer at pH 8.0 containing M_2-AChR overnight (Scheme 2b).

To confirm the successful synthesis of the nanomaterials, the MCM-41 scaffold and solids **S1**, **S2** and **S3** were characterized following standard techniques (see Section 2 and Figures S1–S4 in the Supporting Information). Powder X-ray diffraction (PXRD) of MCM-41 nanoparticles as-synthesized (Figure S1, curve a) shows four low-angle reflections typical of a hexagonal array, indexed as (100), (110), (200), and (210) Bragg peaks, further yielding a cell parameter a_0 of 44.16 Å (distance between planes d_{100} = 38 Å). A significant displacement of 6–8 Å of the (100) peak is then observed in the PXRD pattern of the calcined MCM-41 nanoparticles (Figure S1, curve b), related to condensation of silanol groups in the calcination step. Curve c in Figure S1 shows the **S2** PXRD pattern. Peak intensities decrease and a broadening of the (110) and (200) reflections is found, related to a loss of contrast due to the filling of the pore voids with rhodamine B and surface functionalization. N_2 adsorption-desorption studies of the calcined MCM-41 nanoparticles show a type IV isotherm, typical of mesoporous materials (curve (a) in Figure S2). The absence of a hysteresis cycle in this interval and the shape of the curve suggest the existence of uniform and cylindrical mesopores, with a pore diameter of 1.95 ± 0.05 nm and a total pore volume of 1.18 $cm^3\ g^{-1}$, both calculated by using the BJH model on the adsorption branch of the isotherm. Furthermore, the application of the Brunauer-Emmett-Teller (BET) model results in a value for the total specific surface area of 946.89 $m^2\ g^{-1}$ for the calcined MCM-41. The N_2 adsorption–desorption isotherm of **S2** (curve (b) in Figure S2) is typical of mesoporous systems with partially filled mesopores, for which BET and BJH models indicate a pronounced reduction of the specific surface (16.31 $m^2\ g^{-1}$) and a decrease of pore volume (0.21 $cm^3\ g^{-1}$). From thermogravimetric and elemental analysis studies (Figure S3), contents of 0.25 ± 0.01 and 0.65 ± 0.01 mmol of rhodamine B and bethanechol, respectively, per gram of solid **S2** were calculated (27.9% of organic matter content in **S2**). Moreover, the M_2-AChR content in solid **S3** was determined by BCA Protein assay. An amount of 0.0246 µg of M_2-AChR per milligram of solid was anchored to the outer surface of **S3**. The typical hexagonal porosity of the MCM-41 matrix is clearly visualized through TEM images for all solids obtained. MCM-41 (Figure 1a), and solids **S2** and **S3** (Figure 1b and 1c, respectively) are obtained as spherical particles with an average diameter of 108 ± 6 nm (n = 30 particles), confirming that the siliceous matrix structure remains unaltered after the functionalisation process. To complete the characterization, the different steps for the preparation of the nanosensor were evaluated by zeta potential measurements and dynamic light scattering (DLS) analysis. The zeta potential shows vales of −30.6, –22.0, +2.25 and –12.5 mV for calcined MCM-41, **S1**, **S2** and **S3**, respectively. Additionally, hydrodynamic diameter values of 171 ± 4, 265 ± 7, 292 ± 14 and 765 ± 10 nm were found for the starting MCM-41, **S1**, **S2** and **S3** solids, respectively (Figure 1e). Moreover, functionalization of the nanoparticles was also followed by FTIR analysis (Figure S4). The FTIR spectrum of calcined MCM-41 nanoparticles shows a typical

Please do not adjust margins

absorption band at ca. 1100 related to the bond stretching vibrations of Si-O-Si. Moreover, solid **S3** displays bands at ca. 1629 and 3319 cm^{-1} ascribed to the vibration of peptide bonds and terminal NH_2 and COOH groups from M_2-AChR.

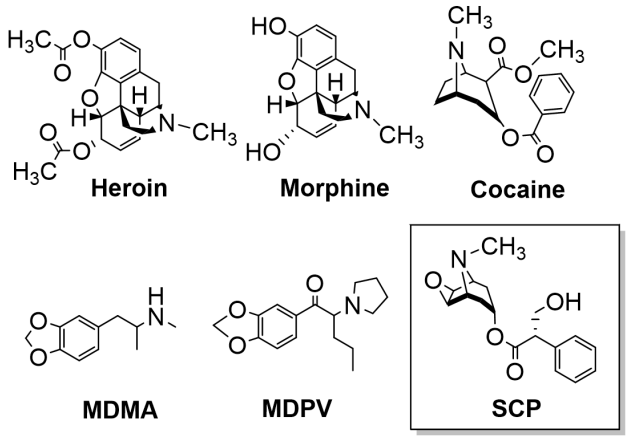

Scheme 3. Structure of different drugs used in the selectivity studies.

Once the nanoparticles were characterized, we studied rhodamine B release from **S3** (1 mg) in 800 µL of Tris-HCl buffer at pH 8.0 in the absence and in the presence of SCP (see section 3 in SI for details). The obtained payload delivery kinetics are shown in Figure 2a. In the absence of SCP, a low cargo delivery is observed, whereas in the presence of SCP a remarkable release of rhodamine B is found. This cargo delivery agrees with M_2-AChR detachment from the surface of the nanoparticles, due to a displacement of the M_2-AChR induced by the presence of SCP. These results are in accordance with the reported higher affinity constant of the M_2 muscarinic receptor for SCP (0.2 ± 0.1 nM) than for bethanechol (13 ± 4 µM). Affinity of M_2-AChR for bethanechol explains the tight pore closure in **S3**, whereas the larger affinity of M_2-AChR for SCP explains displacement of the former from **S3** and cargo release.[34] Finally, to check the crucial role played by M_2-AChR in the SCP-induced rhodamine B delivery from **S3**, a release experiment from uncapped solid **S2** in absence and presence of SCP was carried out. In this case an equally high, uncontrolled release of rhodamine was observed in both cases (Figure S5).

In a further step, the release of rhodamine B from **S3** in the presence of increasing amounts of SCP (from 2.24 to 3150 µM) in Tris-HCl buffer solution at pH 8.0 was evaluated (Figure 2b). The obtained results demonstrate an enhancement of the rhodamine B emission at 572 nm as the SCP concentration increases. From the titration curve, a limit of detection (LOD) of 92 µM is calculated. The maximum oral dosage of SCP for medical purposes is 80 mg in 150 mL of water (264 µM), while 100 mg (330 µM) can be lethal in adults.[39] Hence, the detection limit reached allows to reliably identify SCP with this method. Afterwards, the selectivity of the nanosensor was evaluated in buffer solutions containing other common psychoactive drugs whose consumption is (widely) popular, such as morphine, cocaine, MDMA, heroin and MDPV (Scheme 3). In a typical experiment, the drugs at a concentration of 345 µM were added to suspensions of **S3** and rhodamine B delivery was measured after 2 min. The obtained results are shown in Figure 3. Only the presence of SCP induces a remarkable cargo delivery (set as 100% fluorescence) whereas for the other drugs, rhodamine B release was much less pronounced (less than 30%).

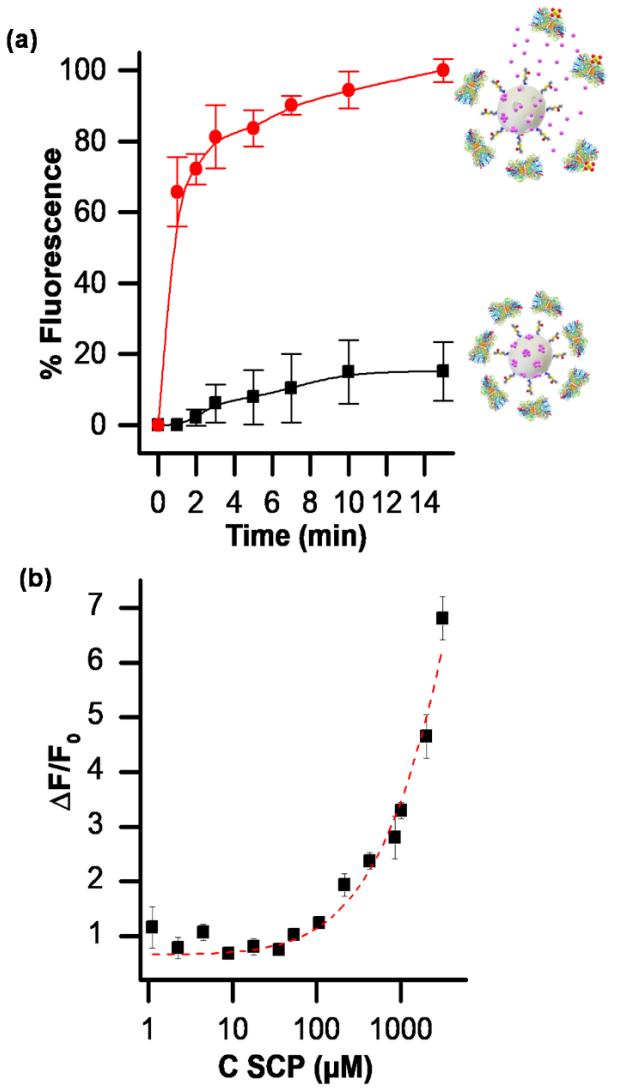

Figure 2. (a) Delivery profiles of rhodamine B from solid **S3** in Tris-HCl buffer at pH 8.0 in absence (black line) and in the presence (red line) of SCP (2.7 mM). (b) Fluorescence intensity of rhodamine B released from solid **S3** in the presence of different amounts of SCP in Tris-HCl Buffer at pH 8.0 after 10 min of addition. Error bars are expressed as 3σ for three independent experiments.

The results indicate that **S3** shows an acceptable selectivity towards SCP to integrate the material with rapid tests. Moreover, these findings agree with the expected poor interaction of the tested drugs and the M_2-AChR receptor. Thus, morphine activates the µ opioid receptors or MU receptors involved in pain sensations, whereas cocaine affects the dopaminergic D1 receptor. In addition, MDPV links to the dopamine active transporter (DAT), blocking dopamine reuptake out of the synaptic cleft whereas the principal mechanism of MDMA-induced euphoria is serotonergic and dopaminergic enhancement. In addition, in vivo SCP causes a maximal increase in acetylcholine levels to 10-12-fold over basal values.[40]

We also aimed to demonstrate the feasibility of the nanosensor to detect SCP in complex competitive medium such as saliva. To this end, similar rhodamine delivery studies from **S3** were performed in saliva diluted to 30% with Tris-HCl buffer at pH 8.0 spiked (or not spiked) with SCP. As illustrated in Figure S6, a significant increase in the fluorescence emission of rhodamine B released from solid **S3**

Please do not adjust margins

Please do not adjust margins

occurs preferentially in the presence of SCP. Furthermore, the sensitivity of **S3** in saliva was measured, showing a detection limit for SCP of 103 µM (Figure S7).

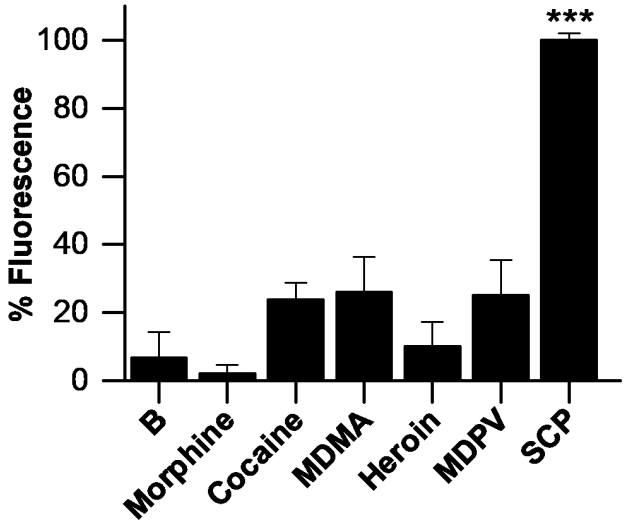

Figure 3. Emission of rhodamine B at 572 nm (λ_{exc} = 565 nm) from a Tris-HCl buffered suspension of solid **S3** in presence of common drugs (345 µM) 2 min after addition. Error bars are expressed as 3σ for three independent experiments (***p < 0.0001).

Encouraged by these results, we moved a step forward with the purpose to obtain a rapid and portable quick test for SCP detection. In areas such as health care, agriculture, environmental monitoring, forensics and food safety preventive and prognostic onsite analyses depend heavily on low-cost point-of-care (POC) or point-of-need tests. Among different technologies, LFAs have become increasingly popular as POC diagnostic tool because of their user-friendliness, specificity, cost-effective and time-saving nature.[41] Furthermore, and very important in terms of the immediate documentation of testing results especially in applications addressing the tracing of illicit drugs, this type of assays can be coupled to smartphone read out.[42,43] In fact, the integration of mobile phones in (bio)sensing devices is impacting the POC field significantly.[31] LFAs could help establish a ubiquitous platform for real-time, on-site analysis. To this end, we proceeded to embed **S3** into a highly selective and sensitive LFA for the direct in situ detection of SCP with a smartphone readout. **S3** was thus integrated into glass fibre membranes previously coated with hydrophobic WAX barriers (**S3-WAX-GF**; see experimental details in section 3.1 in Supporting Information) using an absorbent pad located at the top of the strip, after an optimisation process where different materials and conditions were tested. The strip design consists of two zones, zone A in which the sensing material is deposited at the bottom of the strip and zone B in which the fluorescence signal of the released dye dragged in the solvent flow is collected (Scheme 4). The function of the absorbent pad is to wick the fluid through the membrane through capillary forces. In this way, the released dye can be transported through the membrane, allowing the spatial separation between the nanoprobes and the released dye. When the strip is immersed in a solution that does not contain the target analyte, no signal (or a poor signal) would be recorded in zone B since no release of the entrapped dye from the pores occurs. In addition, the nanomaterial remains in zone A without flowing with the solvent. However, when the strip is dipped

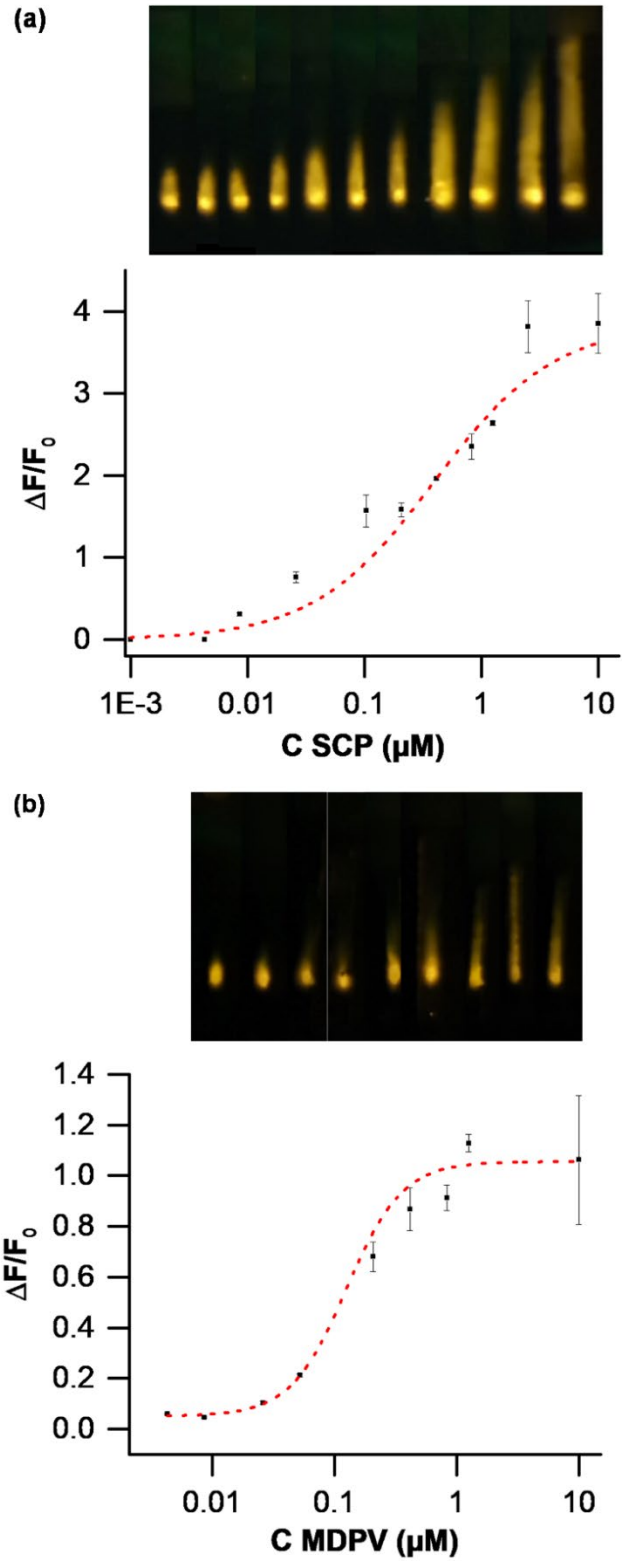

Figure 4. (a) Release of rhodamine B from solid **S3** in the presence of different amounts of SCP in 30% extracted saliva after 10 min of dipping. (b) Release of rhodamine B from solid **S6** in the presence of different amounts of MDPV in 30% extracted saliva after 10 min of dipping. Error bars are expressed as 3σ for three independent experiments. Top: Collage of the photographs registered with the smartphone showing the rhodamine B released in zone B from solid **S3** (a) and solid **S6** (b), shot under proper light excitation.

Please do not adjust margins

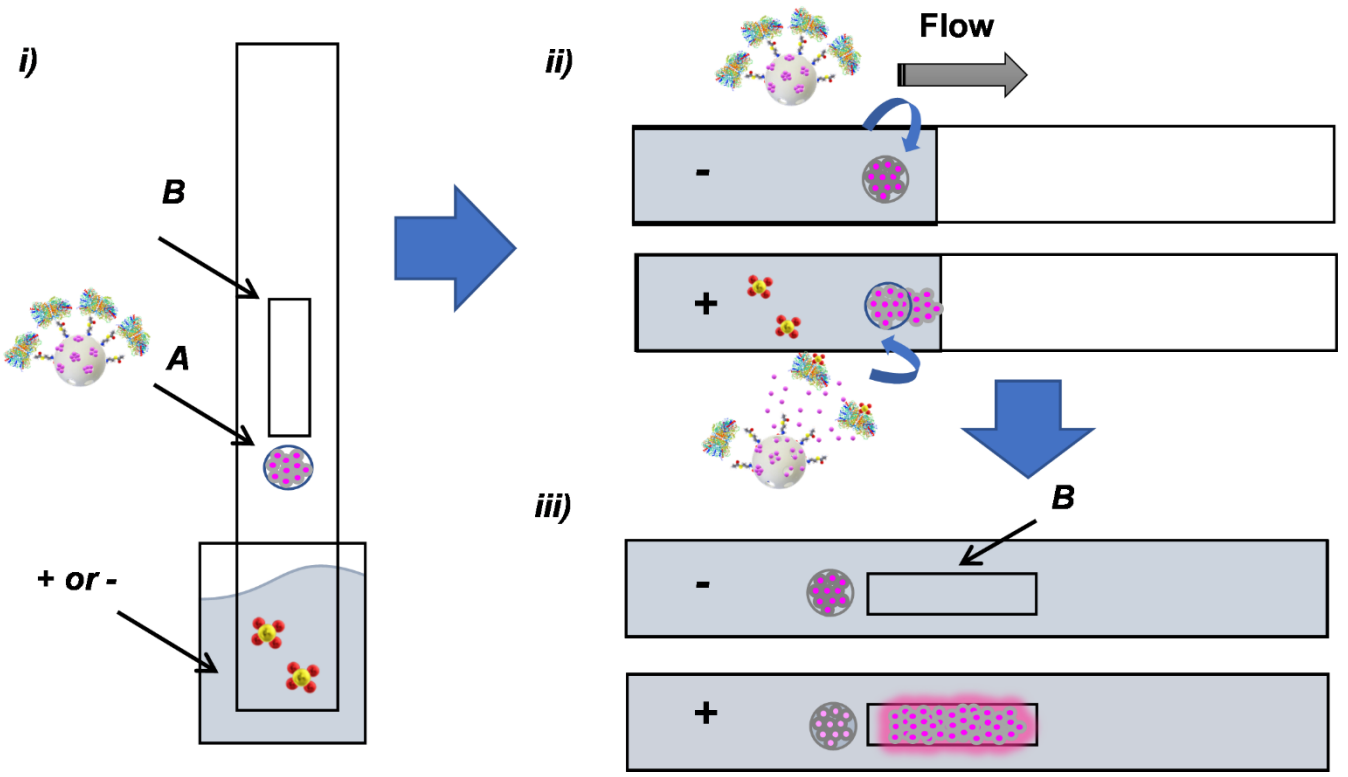

Scheme 4. Design of the lateral flow assay on strip with an **S3-WAX-GF** membrane. i) Schematic of the integration of **S3** in the zone A of the lateral flow strip immersed in the solution potentially containing SCP. ii) No release occurs in the absence of the analyte (negative test), while dye is released in its presence (positive test). iii) Rhodamine B released from solid **S3** only in the presence of SCP is detected in zone B.

in a solution with a specific concentration of SCP, the interaction of the analyte with **S3** results in the delivery of the rhodamine B cargo (*vide ante*). The released dye would flow with the solvent up to zone B where the fluorescence emission can be measured using a smartphone equipped with a 3D-printed case and a strip holder, guaranteeing defined light conditions.[22] By means of this device, rhodamine B release is measured using a 522 nm-LED as excitation source powered by the smartphone via a USB-OTG link and filtered by a short-pass filter (532 nm) while collecting the emission through a long-pass filter (550 nm). Rhodamine B release can thus be correlated to the amount of SCP present in the sample through comparison with a calibration curve.

Following this approach, 2 µL of a buffered suspension of **S3** (1 mg/mL) was deposited in zone A with a micropipette and left to dry for 5 min. Then, the strip was dipped into 75 µL of a buffered solution in the presence and absence of SCP. After 10 min of development and 5 min of drying, the test strips were placed in a holder, the holder inserted into a 3D-printed case fit on the smartphone and a photograph was taken with the smartphone camera. The drying step was found to be essential because varying amounts of residual liquid on the strip influence the fluorescence of the dye. The strips were photographed with the smartphone camera app under proper light conditions (ISO 100 and exposure time of 1/10 s). The fluorescence intensity of the strip photographs was analysed by extracting the integrated fluorescence density of zone B with the software ImageJ.

Based on the lateral flow experiment designed above, we studied the response of **S3-WAX-GF** membranes as a function of the concentration of SCP in Tris-HCl buffer solution. For this purpose, **S3-WAX-GF** membranes (0.5 x 2.5 cm in size) were prepared and dipped into different solutions with increasing concentrations of SCP (from 8.6 µM to 9.99 mM). As can be seen in Figure S8 when the SCP concentration increases a significant enhancement of the fluorescence emission is observed. From the titration profiles, a detection limit of 0.04 µM was calculated. Finally, **S3-WAX-GF** membranes were tested under more realistic conditions and were able to detect SCP in saliva samples with a limit of detection of 18.7 µM (Figure 4a). In addition, other illicit drugs (200 µM) were also assessed in cross-reactivity studies and the results in terms of selectivity were like those observed by using **S3** in solution (Figure S9).

Considering the modularity of the system, a dualplex lateral flow assay for the simultaneous detection of SCP and the "cannibal drug" (MDPV) in saliva samples was developed. For the detection of MDPV, gated nanoprobes **S6** were prepared following procedures previously described by us.[25] **S6** consists of mesoporous silica nanoparticles (MSNs) loaded with the same fluorescent reporter (rhodamine B) and functionalized on the external surface with a dopamine derivative (**5**), which specifically interacts with the recombinant human dopamine transporter (DAT), capping the pores (Scheme S1). Following the same procedure as described above for SCP, aqueous suspension of **S6** (1 mg/mL) were deposited onto **WAX-GF** membranes (0.5 x 2.5 cm size), obtaining **S6-WAX-GF**. These membranes were introduced into different saliva extracted solution (75 µL) with increasing MDPV concentrations (from 2.1 µM to 9.99

mM). From the obtained titration profiles, an LOD of 0.03 µM was calculated (Figure 4b). Moreover, the **S6-WAX-GF** membranes were able to selectively detect MDPV versus MDMA, morphine, heroin, cocaine, MDPV and scopolamine (Figure S10).

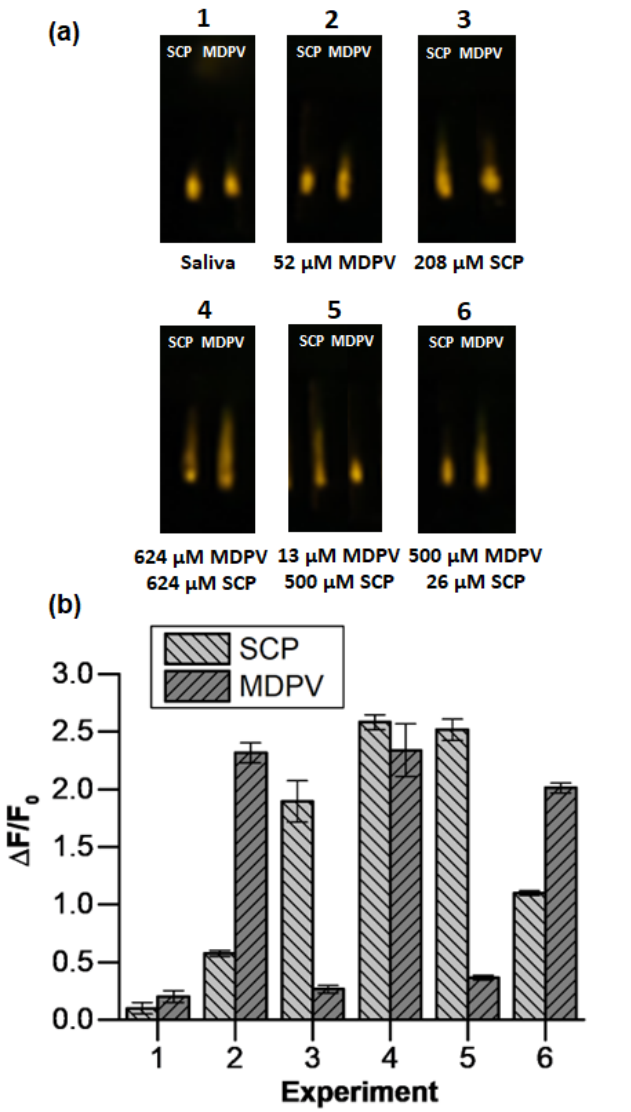

Figure 5. (a) Collage of the photographs registered with the smartphone showing the fluorescence signal of rhodamine B in the detection zone B in the absence and the presence of different concentrations of SCP and the "cannibal drug" in extracted saliva samples. (b) Release of rhodamine B from **S6/S3-WAX-GF** strips in the presence of different amounts of SCP and MDPV extracted saliva after 10 min of dipping. Error bars are expressed as 3σ for three independent experiments.

Considering the design above, a dual-channel strip was prepared using two identical channel patterns wax-printed into the GF membrane with the aim to test for the presence of both drugs SCP and MDPV simultaneously. **S3** was deposited in the first channel of the strip and **S6** in the second channel, using identical procedures as before and yielding **S6/S3-WAX-GF** membranes (Figure S11). The two-channel strip was dipped into different mixed solutions (300 µL) containing various concentrations of the two target compounds and the results obtained are depicted in Figure 5. As can be seen, the dual-channel LFA enables the selective detection of SCP and MDPV in saliva. The studies demonstrated that it is possible to develop a lateral flow assay for the simultaneous detection of different drugs which would be of utmost importance in the areas of forensics, drug control and health monitoring. In fact, multiplexing features are one of the major challenges in this field of onsite rapid analysis.[41] Thus, despite multiplexed detection has been carried out on LFAs, examples to detect small organic molecules are still rare.

Conclusions

We report herein the design, synthesis, and characterization of a rapid, highly selective, and sensitive nanosensor for SCP detection in solution and in saliva simulating a realistic environment. The SCP nanosensor consists of MSNs loaded with a fluorescent reporter (rhodamine B) and functionalized on the external surface with a non-selective muscarinic agonist (bethanechol). M_2-AChR interaction with the anchored bethanechol derivative leads to capping of the pores. The sensing mechanism relies on a M_2-AChR-bethanechol recognition inhibition, with subsequent M_2-AChR detachment after its coordination with SCP and cargo delivery. This was confirmed from kinetic release experiments where a remarkable enhancement in the fluorescence response was only observed in the presence of SCP, which allows diffusion of entrapped dye molecules from the pores when M_2-AChR is displaced. Moreover, the nanoprobe shows a highly sensitivity in buffered solution (LOD of 92 µM) and in a competitive environment such as saliva (LOD of 103 µM). Other drugs (such as cocaine, heroin, morphine, MDMA and MDPV) induce a negligible cargo release. The material was incorporated into strips for lateral-flow assays coupled to smartphone readout without further treatment or conditioning of the test strips while guaranteeing fast overall assay times of <15 min. The assay has fast response time, good selectivity, and exceptional sensitivity, reaching a LOD as low as 0.04 µM in aqueous solution and of 18.7 µM in extracted saliva samples. Finally, a dualplex LFA capable of detecting *in situ* and *at site* both, SCP and the "cannibal drug" MDPV was developed. Considering the sensitivity and selectivity of the assay, this system provides a highly appealing and reliable approach for the development of portable devices with short assay times and easily handling for the accurate detection of different drugs. Taking into account the versatility of the gated material and the modularity of the assay, it is apparent that this generic approach could be easily transferable to the detection of other drugs from liquid samples without the use of specialised personnel or complex instrumentations.

Author Contributions

The manuscript was written through contributions of all authors. All authors have given approval to the final version of the manuscript. E.G., E.C., M.D.M., K. R., F.S. and R.M.M. conceived and designed the research, performed most of the experiments, contributed to the experimental designs, data analysis, discussion, and writing. E.G., and E.C. synthesized and characterized all organic molecules. E.G., E.C. carried out the kinetic studies and lateral flow assays. E.G., E.C., F.S. K. R. and R.M.M. analysed the data. Finally, E.G., E.C., M.D.M.,

Please do not adjust margins

K.R., F.S. and R.M.M. wrote the manuscript with feedback from all the authors.

Conflicts of interest

"There are no conflicts to declare".

Acknowledgements

This research was funded by the Ministerio de Ciencia, Innovación y Universidades (Spanish Government), the Agencia Estatal de Investigación (AEI), the European Union (projects RTI2018-100910-B-C41 and RTI2018-101599-B-C22-AR (MCIU/AEI/ FEDER, EU), the Conselleria de Innovación, Universidades, Ciencia y Sociedad Digital, Generalitat Valenciana (Project PROMETEO 2018/024) and the German Research Foundation (DFG; CL 761/1-19). E. G. is grateful to the Spanish MEC for her FPU grant (FPU16/02464).

References

1 U. Renner, R. Oertel and W. Kirch, *Ther. Drug Monit.,* 2005, **27**, 655-665.
2 M. García, M. Pérez-Cárceles, E. Osuna and I. Legaz, *J. Forensic Leg. Med.* 2021, **79**, 102151.
3 M. Hauw, M. Revranche, V. Kovess-Masfety and M. Husky, *J. Trauma. Stress*., 2021, **34**, 416-426.
4 K. Kohnen-Johannsen and O. Kayser, *Molecules*, 2019, **24**, 796.
5 A. Lakstygal, T. Kolesnikova, S. Khatsko, K. Zabegalov, A. Volgin, K. Demin, V. Shevyrin, E. Wappler-Guzzetta and A. Kalueff, *ACS Chem. Neurosci.,* 2019, **10**, 2144-2159.
6 K. Lusthof, I. Bosman, B. Kubat and M. Vincenten-van Maanen, *Forensic Sci. Int.,* 2017, **274**, 79-82.
7 J. Saiz, T. Mai, M. Lopez, C. Bartolome, P. Hauser and C. Garcia-Ruiz, *Sci. Justice,* 2013, **53**, 409-414.
8 W. Drevets, C. Zarate and M. Furey, *Biol. Psychiatry*., 2013, **73**, 1156-1163.
9 S. Liu, D. Shi, Z. Sun, Y. He, J. Yang and G. Wang, *Front. Psychiatry*., 2021, **12**, 601985.
10 W. Drevets, A. Bhattacharya, M. Furey, R. Du-man and J. Krystal, *In Advances in Pharmacology, Eds. Academic Press: Cambridge*, 2020; **89**, 357-386.
11 R. Oertel, K. Richter, U. Ebert and W. Kirch, *J. Chromatogr. B: Biomed. Sci. Appl.*, 1996, **682**, 259-264.
12 J. Deutsch, T. Soncrant, N. Greig and S. Rapoport, *J. Chromatogr. B: Biomed. Sci. Appl.,* 1990, **528**, 325-331.
13 S. Swaminathan, J. Fisher, N. Brogden and K. Kandimal-la, *J. Pharm. Biomed. Anal.*, 2019, **164**, 41-46.
14 H. Chen, J. Marín-Sáez, R. Romero-González and A. Garrido Frenich, *Food Chem.,* 2017, **218**, 173-180.
15 M. Ribeiro, D. Barreto, J. Flávio da S. Petruci and E. Richter, *Microchem. J.*, 2022, **172**, 106985.
16 M. Gamal, *Analyst*, 2020, **145**, 2025-2037.
17 K. Koczula and A. Gallotta, *Essays Biochem.*, 2016, **60**, 111-120.
18 C. Parolo and A. Merkoçi, *Chem. Soc. Rev.*, 2013, **42**, 450-457.
19 J. Beck, J. Vartuli, J. Higgins, J. Schlenker, W. Roth, M. Leonowicz, C. Kresge, K. Schmitt, C. Chu, D. Olson, E. Sheppard and S. McCullen, *J. Am. Chem. Soc.,* 1992, 10834-10843.
20 P. Diez, E. Lucena-Sanchez, A. Escudero, A. Llopis-Lorente, R. Villalonga and R. Martinez-Manez, *ACS Nano*, 2021, **15**, 4467-4480.
21 A. Garcia-Fernandez, F. Sancenon and R. Martinez-Manez, *Adv. Drug Delivery Rev.*, 2021, **177**, 113953.
22 E. Costa, E. Climent, S. Ast, M. Weller, J. Canning and K. Rurack, *Analyst*, 2020, **145**, 3490-3494.
23 B. Lozano-Torres, J. Blandez, F. Sancenon and R. Martinez-Manez, *Anal. Bioanal. Chem.*, 2021, **413**, 2361-2388.
24 B. de Luis, A. Llopis-Lorente, F. Sancenón and R. Martínez-Máñez, *Chem. Soc. Rev.,* 2021, **50**, 8829-8856.
25 E. Garrido, M. Alfonso, B. Díaz de Greñu, M. Marcos, A. Costero, S. Gil, F. Sancenón and R. Martínez-Máñez, *ACS Sens.* 2020, **5**, 2966-2972.
26 B. de Luis, A. Llopis-Lorente, P. Rincón, J. Gadea, F. Sancenón, E. Aznar, R. Villalonga, J. Murguía and R. Martínez-Máñez, *Angew. Chem. Int. Ed.*, 2019, **58**, 14986-14990.
27 B. de Luis, Á. Morellá-Aucejo, A. Llopis-Lorente, T. Godoy-Reyes, R. Villalonga, E. Aznar, F. Sancenón and R. Martínez-Máñez, *Chem. Sci.*, 2021, **12**, 1551-1559.
28 E. Climent, D. Gröninger, M. Hecht, M. Walter, R. Martínez-Máñez, M. Weller, F. Sancenón, P. Amorós and K. Rurack, *Chem. Eur. J.,* 2013, **19**, 4117-4122.
29 E. Garrido, M. Alfonso, B. Díaz de Greñu, B. Lozano-Torres, M. Parra, P. Gaviña, M. Marcos, R. Martínez-Máñez and F. Sancenón, *Chem. Eur. J.,* 2020, **26**, 2813-2816.
30 F. Sancenón, L. Pascual, M. Oroval, E. Aznar and R. Martínez-Máñez, *ChemistryOpen,* 2015, **4**, 418-437.
31 E. Climent and K. Rurack, *Angew. Chem. Int. Ed.,* 2021, **60**, 26287-26297.
32 L. Bezinge, A. Suea-Ngam, A. DeMello and C. Shih, *Mol. Syst. Des. Eng.,* 2020, **5**, 49-66.
33 C. Parolo, A. Sena-Torralba, J. Bergua, E. Calucho, C. Fuentes-Chust, L. Hu, L. Rivas, R. Alvarez-Diduk, E. Nguyen, S. Cinti, D. Quesada-Gonzalez and A. Merkoci, *Nat. Protoc.,* 2020, **15**, 3788-3816.
34 E. Moreno-Galindo, J. Alamilla, J. Sanchez-Chapula, M. Tristani-Firouzi and R. Navarro-Polanco, *Pfluegers Arch.* 2016, **468**, 1207-1214.
35 K. Katayama, K. Suzuki, R. Suno, H. Tsujimoto, S. Iwata, T. Kobayashi and H. Kandori, *J. Phys. Chem. Lett.,* 2019, **10**, 7270-7276.
36 Q. Cai, Z. Luo, W. Pang, Y. Fan, X. Chen and F. Cui, *Chem. Mater.,* 2001, **13**, 258-263.
37 A. Valla, D. Cartier, F. Zentz and R. Labia, *Synth. Commun.*, 2006, **36**, 3591-3597.
38 E. Largy, W. Liu, A. Hasan and D. Perrin, *ChemBioChem*, 2013, **14**, 2199-208.
39 C. Corallo, A. Whitfield and A. Wu, *Ther. Clin. Risk. Manage.,* 2009, **5**, 719-723.
40 D. Johnson, F. Nedza, D. Spracklin, K. Ward, A. Schmidt, P. Iredale, D. Godek and H. Rollema, *Eur. J. Pharmacol.*, 2005, **506**, 209-219.
41 E. Climent, M. Biyikal, D. Gröninger, M. Weller, R. Martínez-Máñez and K. Rurack, *Angew. Chem. Int. Ed.*, 2020, **59**, 23862-23869.
42 B. Jin, Y. Yang, R. He, Y. Park, A. Lee, D. Bai, F. Li, T. Lu, F. Xu and M. Lin, *Sens. Actuators, B,* 2018, **276**, 48-56.
43 W. Xiao, C. Huang, F. Xu, J. Yan, H. Bian, Q. Fu, K. Xie, L. Wang and Y. Tang, *Sens. Actuators, B*, 2018, **266**, 63-70.

Please do not adjust margins